Projectile and target scaling of the total ionization cross sections of atoms and molecules

E. C. Montenegro,[1] G. M. Sigaud,[2] and R. D. DuBois[3,*]

[1]*Instituto de Física, Universidade Federal do Rio de Janeiro, Caixa Postal 68528, Rio de Janeiro, RJ 21945-970, Brazil*

[2]*Departamento de Física, Pontifícia Universidade Católica do Rio de Janeiro, Caixa Postal 38071, Rio de Janeiro, RJ 22452-970, Brazil*

[3]*Department of Physics, Missouri University of Science and Technology, Rolla, Missouri 65409, USA*

(Received 16 November 2012; published 16 January 2013)

A scaling for the total ionization cross sections of atomic and molecular targets by neutral to highly charged projectiles with energies ranging from a few keV/u to many MeV/u is presented, with few free parameters, all velocity independent, and whose values do not vary appreciably for the projectiles and atomic and molecular targets considered here. Another important feature of the proposed scaling is that it has been built considering the characteristics of the collision systems, taking into account the various physical processes that lead to target ionization and the velocity regions where each of them dominates, and performing a smooth transition between them. This scaling describes quite well the existent experimental data covering a broad range of collision systems as diverse as H^+ on H, Xe^{30+} on He, or O^{6+} on uracil.

DOI: 10.1103/PhysRevA.87.012706 PACS number(s): 34.50.Fa, 52.20.Hv

I. INTRODUCTION

Electron, proton, or heavy-particle ionization plays a major role in the modeling of several processes connected to plasma and atmospheric physics as well as in understanding and modeling the damage induced by swift ions (or electrons) penetrating solids or biological media. Generally the interest is in knowing the types and numbers of collision products that are produced plus how much energy is deposited during each interaction between the projectile and target. However, since each particular field has its own specialized needs one requires such information for a virtually endless number of systems and energies. In astrophysics, for instance, the primary interest is in interactions between fully stripped, low atomic number ions and atoms or simple molecules, whereas for atmospheric physics, the interest is in interactions between protons and dressed low atomic number ions and simple molecules. For plasmas, industrial uses primarily involve low- to medium-charged keV ions, in contrast, high-energy-density research studies use high-energy highly charged ions ranging from α particles to very heavy ions. For dosimetry and medical uses, knowledge about keV to MeV light ions interacting with bulk materials or biosystems is important. Information about inelastic interactions is also essential in the design and operation of high-energy accelerators and storage rings. This means that the systems of interest cover the whole periodic table of atoms, plus simple to complex molecules, while the projectile charge states range from -1 to fully stripped, including 0; and the energies range from a few keV to hundreds of MeV/u.

To obtain all the required information is a very complicated—if not impossible—task, since singly and/or multiply ionized particles can be produced, and several processes such as pure target ionization, electron capture by the projectile, and projectile electron loss can all occur with their relative importance depending on the projectile velocity and charge state and on the target species. Because of this wide application, scaling laws where a large number of systems can be modeled through the knowledge of a small number of parameters are useful if not essential.

For target ionization, numerous attempts have been made over the decades to find a general scaling law for the total ionization of (any) target by (any) projectile. However, one is challenged by several very difficult problems, one of which is that, depending on the projectile velocity and charge state, the ionization process spans three collision regimes where quite different interaction processes and dynamics dominate. At high velocities, where q/v—the projectile charge divided by its velocity—is small, perturbation methods apply. Here, the accepted scaling is to plot σ/q^2, where σ is the cross section, versus the impact energy E (Bohr scaling) [1] or versus $\ln(E)/E$ (Bethe-Born scaling) [2]. In the intermediate velocity regime, first-order Bohr scaling breaks down because q/v increases. This is illustrated in the upper portion of Fig. 1, where experimental cross sections for total (single + double) ionization of helium by various bare and highly charged projectiles—namely, H^+ [3,4], He^{2+} [3], Li^{3+} [3,5], B^{5+}, C^{6+}, O^{8+} [6], Ar^{16+} [7], and $I^{5+\,\text{to}\,27+}$ [8]—divided by q^2 are plotted as a function of E/M, the collision energy divided by the projectile mass. Here, higher-order theories must be used and especially for very highly charged projectiles, violation of unitarity for the first-order ionization probabilities, i.e., saturation effects, must be taken into account. In this region, a scaling based on that proposed by Olson and co-workers [9–11] for the electron loss of heavy, highly stripped ions, where σ/q is plotted versus v^2/q, is often used. But, as seen in the middle portion of Fig. 1, where the same data, divided by q, is plotted as a function of $(E/M)/q$, this scaling too breaks down at low impact velocities. A similar breakdown of this Olson scaling for $v^2/q \lesssim 100$ keV/u was recently observed by Illescas *et al.* in the calculated electron production cross sections of the water target by bare ions [12]. Recently [13], we have shown that this breakdown at low velocities is significantly reduced, at least for highly charged ion impact on hydrogen and helium, if the Olson scaling is modified plotting $\sigma/q^{4/3}$ versus $(E/M)/q^{2/3}$. This is illustrated by the bottom portion of Fig. 1.

A third regime, occurring for impact energies below $\sim$100 keV/u, is where electron capture processes become competitive, or dominant, with respect to pure ionization

*dubois@mst.edu

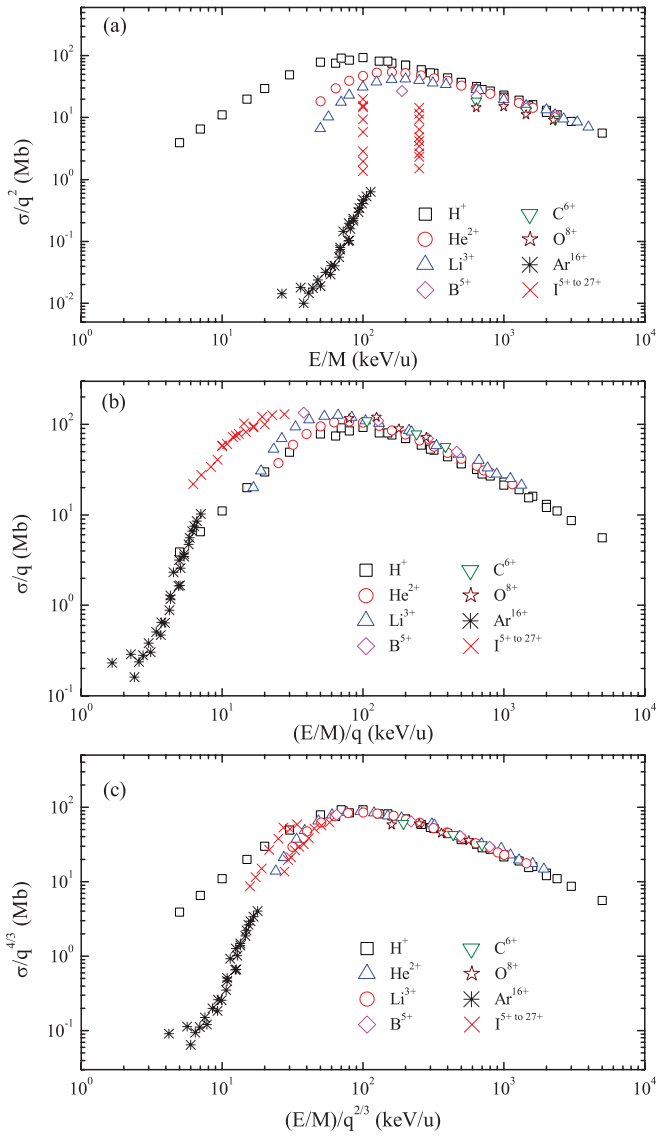

FIG. 1. (Color online) Scaled total (single + double) ionization cross sections of He by bare projectiles. (a) Born scaling: σ/q^2 in Mb versus E/M in keV/u; (b) Olson scaling: σ/q in Mb versus $(E/M)/q$ in keV/u; (c) Scaling from Ref. [13]: $\sigma/q^{4/3}$ in Mb versus $(E/M)/q^{2/3}$ in keV/u. Experiment: black squares, H^+ from Refs. [3,4]; red circles, He^{2+} from Ref. [3]; blue up triangles, Li^{3+} from Refs. [3,5,6]; magenta diamonds, B^{5+}; green down triangles, C^{6+}; and brown stars, O^{8+}, all from Ref. [6]; black asterisks, Ar^{16+} from Ref. [7]; and red crosses, $I^{5+\,\text{to}\,27+}$ from Ref. [8].

processes. Thus, the loss of available flux from the ionization channel due to the capture channel must be taken into account.

Empirical models, such as those introduced by Gillespie [14], for the ionization of atomic H targets in the high- to intermediate-velocity regime, or Wu *et al.* [7,15], for the ionization of He in the intermediate- to low-velocity region, have been proposed. For additional information about these and other scaling methods for the ionization of light targets, such as H and He, the reader is referred to a recent paper by Kaganovich *et al.* [16]. It should be noted at this point that these scalings are essentially projectile scalings and do not directly address the behavior of the ionization cross sections for different targets.

The second challenge relates to neutral and partially stripped ion impact. In this case, one needs to accurately determine both the partially screened projectile nuclear charge q_{scr} and the number of active (projectile electrons which directly interact and ionize target electrons), N_{act}. Here, as outlined by Bates and Griffing [17], the cross sections scale as $q_{\text{scr}}^2 + N_{\text{act}}$, both of which depend on the projectile charge state and velocity. For projectile ionization, we recently proposed methods applicable for determining these values for neutral atoms and molecules ionizing fast, heavy ions [18]. But, for target ionization, although it is possible to use first-order principles to determine q_{scr} and N_{act} in simple systems (see, for example, DuBois and Manson [19]), no method exists for an arbitrary collision system and energy. The effective projectile nuclear field on the target electrons may change appreciably with the collision velocity, so that reasonable estimates of the screening of the projectile charge become very important in the determination of the ionization cross sections.

The third challenge relates to multiple electron transition processes. These include multiple outer-shell ionization, inner-shell ionization followed by various relaxation processes, and capture plus ionization (transfer-ionization) processes. Thus, the determination from first principles of reasonably reliable cross sections for any arbitrary collision system and energy is almost an impossible task.

All this considered, it does not seem to be possible to take into account all the competing processes, mainly those which are more relevant for low-energy collisions, and covering a huge range of projectile charge states with scalings which rely on only one function of q and v, an assumption which is behind the scalings presented in Fig. 1.

As already mentioned, there are many important applications where the production of ions along the track of a swift projectile traversing a medium is crucial information. For example, in hadron-based cancer therapy, a high-energy, highly charged or fully stripped ion (such as C) penetrates the human body. Along its track, the projectile not only deposits energy but, concomitantly, changes its charge state. Starting from typically 400 MeV/u C^{6+} ions at the skin surface, the beam reaches the tumor location with an energy around the maximum of the Bragg peak (~400 keV/u), where the energy deposition is highest, and a charge state around 3. Shortly after, the projectile virtually stops as a neutral particle [20]. Thus, along their paths, the particles in the impinging beam interact with the molecules of the intervening tissues and the ionization processes basically scan the three different regimes pointed out above. Initially, one has a highly charged fast ion; thus, in this region, the ionization can, in principle, be treated using first-order methods. However, the strong field of the projectile may lead to second-order processes, such as saturation. As the projectile energy decreases, the competition with electron capture complicates the description of the ionization, due to the coupling between these two channels. At low energies, the average charge state of the projectile decreases, which means that the ionization occurs in a strongly screened nuclear field.

Some years ago, Montenegro and co-workers devised a target scaling law for the ionization of noble gases by protons, electrons, and He^+ ions based on the plane-wave Born

approximation (PWBA) [21]. Spurred by our recent successes in describing the scaling for projectile ionization by various neutral targets [18] and this target scaling for proton impact [21], here we attempt to empirically extract a universal curve for target ionization by neutral to highly charged projectiles with energies between a few keV/u and several MeV/u. In the following sections, we will present the evolution of this empirical scaling law, beginning with bare-ion−simple-target systems, and progressively including projectiles ranging from neutral to highly charged, ionizing heavier and more complex atomic and molecular targets.

Our goal is to provide a simple scaling model which can be applied not only for modeling purposes but also can be used as a guide in checking theoretical models for multiple ionization, which are presently quite scarce in the literature. The article is organized as follows. In Sec. II, a target scaling applicable for intermediate- to high-velocity proton impact on any target is presented, based on the ionization cross sections within the PWBA. In Sec. III, we develop a scaling model for ionization of He by projectiles having arbitrary charge states ranging from fully stripped to neutral. In Sec. IV, we extend this scaling to many-electron atomic and molecular targets. In Sec. V the present results are summarized and conclusions are drawn. And, in the Appendix, a sample calculation is presented in order to help the reader to follow all the paths leading to the proposed scaled ionization cross section.

II. TARGET SCALING FOR PROTONS

In the case of ionization by light charged particles, in the intermediate- to high-velocity regime, the behavior of the ionization cross section is conveniently described by first-order models, such as the PWBA [2]. Within this approximation, the cross section scales with the projectile charge state as q^2 and with the projectile velocity v as $\sim \ln(v^2)/v^2$ (Bethe-Born scaling) for sufficiently high velocities.

The dependence of the ionization cross section with the target, on the other hand, is not straightforward. As has been shown by several authors (see [19,22,23], and references therein) single ionization of multielectron atoms involves mostly the weakly bound electrons. This means that, when the periodic table of elements is scanned, electrons belonging to atomic outermost shells, with different quantum numbers and described by quite different wave functions, are the main actors for the ionization process. Furthermore, although single ionization is the dominant process, multiple ionization is always present. For light targets such as He, multiple ionization contributes less than 5% to the total ionization cross section. In contrast, for heavier targets such as Kr or Xe, the contribution is on the 20%–30% level [22,24].

For example, the cross section for m-fold ionization, in which m out of a total of N equivalent electrons in the nl subshell undergo transitions with the same probability $P(\vec{b})$ as a function of the impact parameter $\vec{b}$, which is the simplest case possible, is given by [25,26]

$$\sigma^m = \binom{N}{m} \int P(\vec{b})^m [1 - P(\vec{b})]^{(N-m)} d\vec{b}. \tag{1}$$

Thus, the total ionization cross section, $\sigma_{\mathrm{T}}^{\mathrm{ion}}$, can be written as the sum of all the partial m-fold ionization cross sections, $\sigma_{\mathrm{T}}^{\mathrm{ion}} = \sum_m \sigma^m$. On the other hand, many experiments do not distinguish between the ionization from different shells and only the sum of the ionization cross sections for each individual subshell nl, σ_{nl}—that is, $\sigma_{\mathrm{T}}^{\mathrm{ion}} = \sum_{nl} \sigma_{nl}$—is available.

Montenegro *et al.* have presented a scaling law for the total ionization for light, single-charged projectiles impinging on noble gases [21]. The starting point of the scaling proposed by these authors was the well-known expression for the ionization cross section of an electron occupying a subshell nl by a pointlike projectile, in the high-velocity limit, namely [2,27],

$$\sigma_{nl} = \frac{8\pi q^2 a_0^2 c_{nl} Z_{nl} \ln(2mv^2/D_{nl})}{(I_{nl}/R_\infty)(v/v_0)^2}. \tag{2}$$

In this equation, the constant c_{nl} is the dipole matrix element between the nl orbital and the continuum, summed over all the allowed continuum states, and is the factor which, together with the ionization energy I_{nl}, characterizes the initial electron state. The parameters a_0 and v_0 are the Bohr radius and velocity, respectively, and Z_{nl} is the number of electrons in the nl orbital. D_{nl} is a parameter approximately proportional to I_{nl}.

The scaling presented was based on the fact that the dipole matrix element c_{nl} is pretty much constant ($\sim$0.13) for the np orbitals of atomic hydrogen [2]. With the exception of He, the outermost electrons of noble gases are np-type orbitals; thus, the dipole matrix elements c_{nl} are target independent. It can be easily seen from Eq. (2) that the reduced cross section $I_{nl}^2 \sigma_{nl}/Z_{nl}$ is essentially a function of v^2/I_{nl}, since the logarithm term varies more slowly with v^2 and $q = 1$ for protons. However, this parametrization is not enough to make the calculated ionization cross sections for atomic p orbitals with different values of n coalesce, due to the fact that the c_{nl}'s are not really constant. Those authors introduced a parameter δ_{nl}, of order of unity, which takes into account the small peculiarities of the dipole matrix element associated with the various atomic orbitals. Then, they obtained an excellent coalescence among the cross sections for all np orbitals, including the $1s$ orbital as well, giving rise to a universal curve for this set of orbitals. This can be seen in Fig. 2, where the scaled cross section, with the inclusion of the parameter δ_{nl}, is plotted as a universal function of the collision velocity squared E/M in keV/u divided by the ionization energy of the initial electron state I_{nl} in atomic units. The data include ionization cross sections of H [28] and noble gas atoms [4,22,24,29–31], and, as an extension of the previous work, of several molecules—namely, H_2 [29,32], N_2 [29], H_2O [33], CH_4 [29,34], and uracil ($C_4H_4N_2O_2$) [35]—by protons. It should be remarked here that the great majority of the molecules of our carbon-, nitrogen-, and oxygen-based life have p-orbital bondings. The scaled cross section for singly charged projectiles thus plotted is written as.

$$\frac{\sigma_{nl} I_{nl}^2}{Z_{nl}\delta_{nl}} = F((E/M)/I_{nl}), \tag{3}$$

where the universal function $F((E/M)/I_{nl})$ can be represented by the function

$$F(x) = \frac{A\ln(1 + Bx)}{x} - \frac{AB}{(1 + Cx)^4}, \tag{4}$$

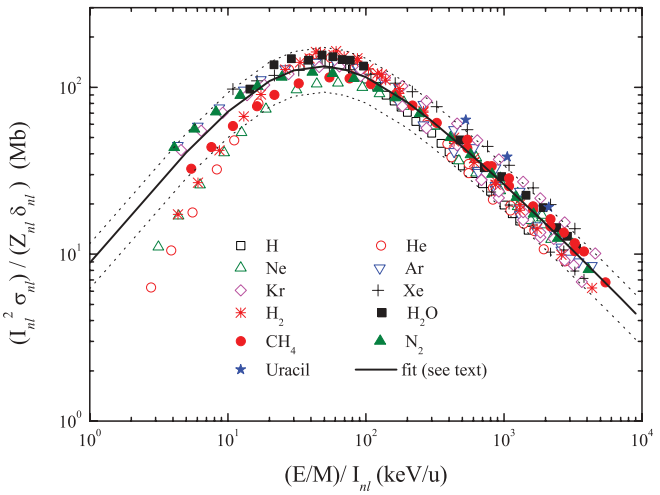

FIG. 2. (Color online) Scaled total ionization cross sections [given by Eq. (3)] of atomic and molecular targets by protons in Mb as a function of the scaled energy $(E/M)/I_{nl}$ in keV/u. Experiment: black open squares, H from Ref. [28]; red open circles, He; green open up triangles, Ne; blue open down triangles, Ar; and magenta open diamonds, Kr, all from Refs. [22,24,29]; black crosses, Xe from Refs. [24] and [30,31] as cited by Rudd [4]; red asterisks, H_2, from Refs. [29,32]; green solid up triangles, N_2, from Ref. [29]; black solid squares, H_2O, from Ref. [33]; red solid circles, CH_4, from Refs. [29,34]; and blue solid stars, uracil, from Iriki *et al.* as cited by Galassi *et al.* [35]. The solid line is the scaling function given by Eq. (4) and the dotted lines represent a deviation of ±30% of the solid line (see text).

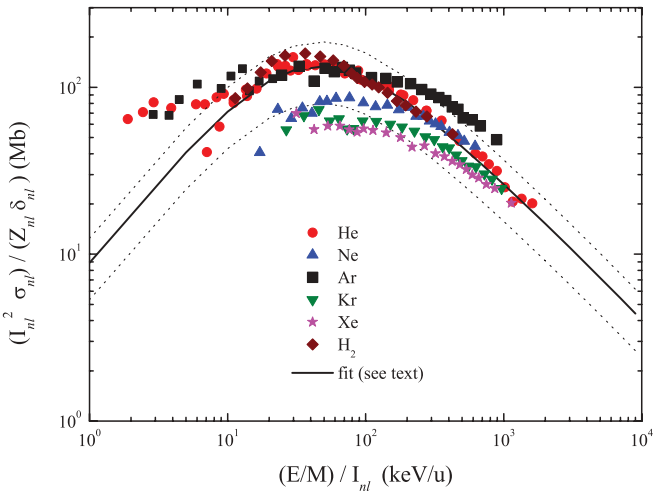

FIG. 3. (Color online) The same as in Fig. 2 for antiprotons. Experiment: red circles, He from Refs. [39–41]; blue up triangles, Ne from Ref. [42]; black squares, Ar from Refs. [41,42]; green down triangles, Kr, and magenta stars, Xe, both from Ref. [42]; and brown diamonds, H_2 from Ref. [40]. The solid line is the scaling function given by Eq. (4) and the dotted lines represent a deviation of ±40% of the solid line (see text).

with $A = 6.15 \times 10^3$, $B = 7.0 \times 10^{-2}$, and $C = 1.4 \times 10^{-2}$ for σ_{nl} in Mb.

The parameters δ_{nl}, Z_{nl}, and I_{nl} used in the scaling for the various targets are shown in Table I. The ionization energies of the outer-shell electrons of the noble gases were taken from [36], while those of the valence molecular orbitals of the molecular targets were those presented by Hwang *et al.* [37], with the exception of uracil. For this molecule, we considered its 11 outermost molecular orbits, which have energies ranging from 9.46 to 15.4 eV, as recently reported by Holland *et al.* [38]. Actually, the scaling shown in Fig. 2 has been made using for σ_{nl} the ionization cross sections taken from experiments which, in general, do not select the original subshell of the electron(s) ejected from the target. Thus, for δ_{nl} and I_{nl} we have used values which were averaged over the outermost subshells whose ionization energies have close values (as, for example, in the case of the 11 outermost orbitals of uracil), and for Z_{nl} the total number of electrons of these subshells.

It can be seen that the proposed function provides a remarkably good scaling for targets ranging from the simple H atom to the complex uracil molecule, within a deviation of ±30%, represented by the dotted lines which accompany the fitted curve $F(x)$ given by Eq. (4). This scaled ionization cross section will, then, be the starting point for the developments which follow.

The same scaling has been used for the target ionization by antiproton projectiles and the results are shown in Fig. 3. The targets are noble gases (He to Xe), from Refs. [39–42], and the H_2 molecule is from Ref. [40]. Even though, in this case, polarization effects are the opposite of those for proton projectiles, we have chosen to use in the scaling for antiprotons the same parameters as those used for protons. Although the dispersion of the data is significantly larger than in the proton case, which impairs further refinements of the scaling, most of the scaled cross sections lie within ±40% of the fitted curve $F(x)$ given by Eq. (4).

III. PROJECTILE SCALING FOR THE He TARGET

From this point on, we will extend the preceding scaling to other projectiles, first concentrating on the He target, since the amount of experimental data for ionization cross sections for this atom far exceeds the available data for any other.

TABLE I. Average values of the parameters δ_{nl}, Z_{nl}, and I_{nl} (a.u.) used in the scaled ionization cross sections, Eq. (3), of atomic and molecular targets by protons (see text).

	H	He	Ne	Ar	Kr	Xe	H_2	N_2	H_2O	CH_4	Uracil
δ_{nl}	0.66	0.8	0.55	0.55	1.21	1.33	1.0	1.0	0.77	1.0	0.5
Z_{nl}	1	2	6	6	6	6	2	6	6	6	22
I_{nl}	1	1.81	1.7	1.18	1.09	0.92	1.15	1.22	1.18	0.92	0.97

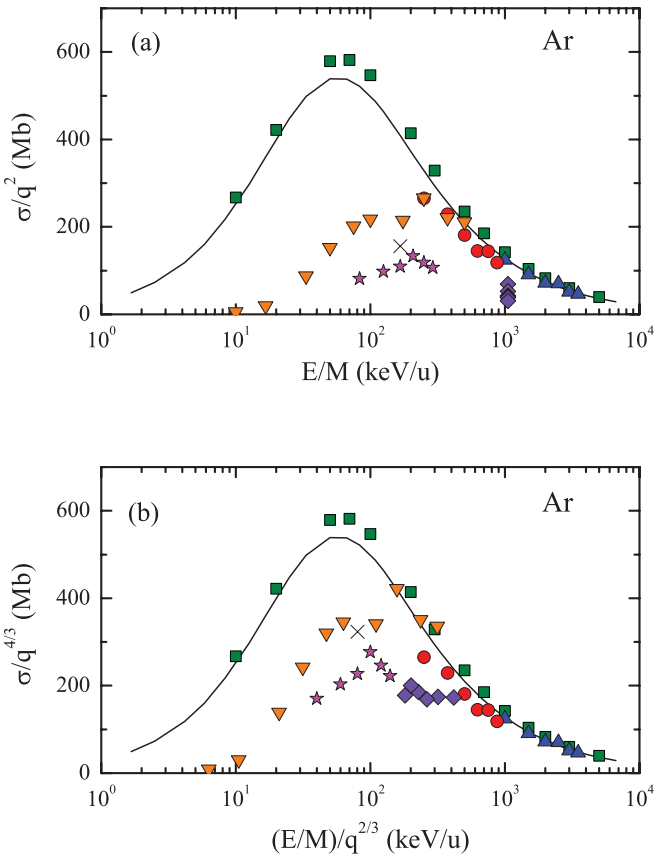

FIG. 4. (Color online) Scaled total ionization cross sections of Ar, in Mb, for various projectiles. (a) Born scaling: σ/q^2 in Mb versus E/M in keV/u; (b) scaling from Ref. [13]: $\sigma/q^{4/3}$ in (Mb) versus $(E/M)/q^{2/3}$ in keV/u. Experiment: green squares, H^+ from Ref. [4]; blue up triangles, H^+ from Ref. [24]; red circles, He^+ from Ref. [43]; orange down triangles, He^{2+} from Ref. [44]; magenta stars, C^{3+} from Ref. [45]; black cross, C^{3+} from Ref. [46]; and violet diamonds, Ar^{q+}, with q ranging from 6 to 14, from Ref. [47]. The solid line is the scaling function given by Eqs. (3) and (4).

A. High- to intermediate-velocity collisions

Several attempts have been made during the past decade in order to find a scaling for target ionization by highly charged projectiles (see, for example, the review of Kaganovich *et al.* [16] for simple, low-Z targets, and references therein). The most obvious procedure is simply to include a scaling which depends on the projectile charge state q, like the Born scaling (σ/q^2 versus v^2), the Olson scaling (σ/q versus v^2/q), or the one proposed in Ref. [13] ($\sigma/q^{4/3}$ versus $v^2/q^{2/3}$).

These simple scalings work quite well for high-velocity bare ions (as long as their charge state is not very high—see Fig. 1), but fails both for partially dressed ions and in the intermediate- and low-velocity regimes. As an example, we show in Fig. 4 the Born scaling and the one proposed in Ref. [13] for the ionization of Ar atoms by bare and dressed projectiles, ranging from protons up to Ar^{14+} ions [43–47]. The curve is that given by Eq. (3). It can be readily seen that neither scaling provides a good description of the experimental data either for highly charged ions or in the intermediate-velocity region, the one proposed in Ref. [13] being better for intermediate velocities, but still not good enough.

In order to try to find a scaling law for the ionization of atomic hydrogen by intermediate-velocity highly charged projectiles within the plane-wave Born approximation (PWBA), Gillespie proposed the inclusion of an exponential factor which is velocity- and charge-state dependent [14]. His scaled ionization cross section, here called σ_G, is given by (from here on the ionization cross section by protons will be called σ_p)

$$\sigma_G = q_G^2 \sigma_p, \tag{5}$$

where

$$q_G = q e^{-f(v,q)} \tag{6}$$

is a parameter which depends on the collision velocity and on the projectile charge state. In the scaling proposed by Gillespie, the function $f(v,q)$ is given by

$$f(v,q) = \lambda q / v^2, \tag{7}$$

where λ is a constant.

B. Intermediate- to low-velocity collisions

Although providing good results for the ionization of hydrogen atoms by H^+, He^{2+}, Li^{2+}, Li^{3+}, C^{4+}, N^{5+}, N^{+4}, and O^{5+} ions, this scaling from Gillespie is subject to several restrictions. First, since the projectile is treated as a structureless pointlike particle, one must have $q \geqslant Z_P/2$, where Z_P is the projectile atomic number [14]. Another restriction is that the calculations are limited to collision velocities larger than 30 keV/u [14]. Actually, the scaled cross section proposed by Gillespie tends to zero faster than the experimental evidence, as the velocity decreases.

Also, Gillespie scaling totally fails for neutral projectiles, since, by keeping the q^2 scaling, it predicts that the ionization cross section is zero, a fact that is definitely not supported by experiment. Actually, there are several sets of data which show that the ionization cross sections by neutral projectiles can be of the same order—or, sometimes, even higher—than those for charged ions (see, for instance, the works of Luna *et al.* for H^+ and H^0 projectiles on water [33], DuBois and Toburen for neutral and singly charged He, C, N, and O projectiles on He [48], and Alvarado *et al.* for neutral and singly charged H, He, and C projectiles on adenine [49]).

The scaling proposed in Sec. II for σ_p by low-Z singly charged projectiles works very well for a wide range of projectile velocities (see Fig. 2). However, if one makes $q = 1$ in Eq. (7), Gillespie's scaled cross section, given by Eq. (5), will differ from the proton cross section σ_p by a velocity-dependent exponential factor which, although tending to 1 at high velocities, may be quite relevant in the intermediate- and low-velocity regimes.

Thus, to circumvent the difficulties pointed out above, we have introduced some modifications in the function $f(v,q)$, given by Eq. (7), but keeping asymptotically the same velocity dependence of the Gillespie scaling, so that it is now written as

$$f(v,q_{scr}) = \frac{\lambda\beta(q_{scr}-1)}{\beta v^2/(2I_{nl}) + \lambda(q_{scr}-1)e^{-2(v^2/2I_{nl})^{3/4}}}, \tag{8}$$

where I_{nl} is the ionization energy of an electron belonging to the outermost target subshell in atomic units, q_{scr} is the

effective screened nuclear charge of the projectile acting on the target active electrons, and β is a parameter given by

$$\beta = \frac{Z_{nl}}{5I_{nl}}\frac{q_{\rm scr}}{Z_{\rm P}}. \tag{9}$$

The parameter λ for He has, of course, a different value than that for H, as given by Gillespie [14]. In fact, λ will be considered a target-dependent fitting parameter in the present scaling procedure, as will be seen later.

The reason for the introduction of this $q_{\rm scr}$ is twofold. First, one has to take into account the fact that, for a dressed projectile, the nuclear field is screened by its electrons. This screening depends on the impact parameter of the collision and becomes more important for intermediate and low velocities. For high velocities—that is, a region dominated by large impact parameters—the target electrons interact essentially with the projectile charge q. Thus, this screened charge has to satisfy the asymptotic conditions: $q_{\rm scr} \to q$ as $r \to \infty$ and $q_{\rm scr} \to Z_{\rm P}$ as $r \to 0$. Using the Hartree-Fock-based analytical screening function from Salvat *et al.* [50], one can write an expression for $q_{\rm scr}$, which has the correct asymptotic behavior, as

$$q_{\rm scr} = q + (Z_{\rm P} - q)\sum_i A_i(1+\alpha_i r_{\rm adiab})e^{-\alpha_i r_{\rm adiab}}, \tag{10}$$

where α_i and A_i are parameters tabulated in Ref. [50], with $\sum_i A_i = 1$.

In Eq. (10), we have considered the distance r as the adiabatic radius $r_{\rm adiab}$, which can be used to define a typical distance for the direct-impact ionization process, being proportional to the collision velocity and inversely proportional to the target electron ionization energy, and is given in atomic units by [51]

$$r_{\rm adiab} = \gamma\frac{2v}{I_{nl}}. \tag{11}$$

In Eq. (11), the factor γ has been used to take into account the different "sizes" of the atomic and molecular targets. The values of γ considered here were 0.8 for He and Ne, 1.0 for the other atomic targets, and 1.4 for the molecular targets.

The second reason concerns the fact that both the Gillespie and Wu scalings go to 0 for neutral projectiles, while the experimental cross sections do not. If one uses $q = 0$ in Eq. (10), one still gets a scaled cross section equal to 0 in the high-velocity regime, when $r_{\rm adiab}$ is high. In order to circumvent this difficulty, we have used in Eq. (10) for neutral projectiles an asymptotic charge $q = q_{\rm asym}$, which is defined as the square root of the ratio between the ionization cross sections by the neutral projectile and by protons at high velocities. Using experimental data for the ionization of He, $q_{\rm asym}$ varies from $\sim$0.6 for H^0 to $\sim$1.5 for Ne^0 impact. For high-velocity charged projectiles, although the main contribution to target ionization comes effectively from large impact parameters, one cannot neglect completely the contribution from small impact parameters. For neutral projectiles, on the other hand, the contribution from distant collisions is very small and ionization is dominated by small impact parameters. Thus, the asymptotic charge reflects somehow the effect of the screening of the projectile nuclear charge by its electrons for high collision velocities, in analogy with the screening contribution to the projectile electron loss process [52].

This modified function $f(v,q_{\rm scr})$, given by Eq. (8), thus tends to 0 as $q_{\rm scr}$ is 1, as for proton impact, but has the same velocity dependence of the Gillespie scaling, as given by Eq. (5), in the high-velocity regime. This has been done on purpose since, at low velocities, $f(v,q_{\rm scr})$ tends to a constant, β. The dependence of the effective charge $qf(v,q_{\rm scr})$ with q and v at low velocities has to include other mechanisms which may lead to target ionization, and which are not properly described by the function given by Eq. (8). This will be discussed in the next section.

C. Low-velocity collisions

Wu *et al.* [7] proposed a scaling law for the ionization of He by highly charged projectiles in the low-velocity region, which works quite well for projectile velocities below 1.5 a.u., but does not match that of Gillespie for intermediate velocities. The scaling proposed by Wu *et al.* also contains an exponential term which, however, has a different dependence on the projectile velocity v and charge state q than Gillespie's: it is a function of the ratio $(v/q^{1/4})$. This scaled cross section, which will be called $\sigma_{\rm W}$, is given by

$$\sigma_{\rm W} = qD(v/q^{1/4})e^{-K/(v/q^{1/4})}, \tag{12}$$

where D and K are fitting parameters, which are given by Wu *et al.* as 1.1×10^4 Mb and 7.24, respectively, for v in atomic units. Since the ionization cross section $\sigma_{\rm p}$ at low energy, as given by Eqs. (3) and (4), depends on the collision velocity as v^2, one can write

$$q^{1/2}\sigma_{\rm p} \propto q^{1/2}v^2 \propto \left(\frac{v}{q^{1/4}}\right)^2, \tag{13}$$

so that the combination of the Wu scaling with the ionization cross section for singly charged projectiles would essentially be proportional to $q^{1/2}\sigma_{\rm p}$.

However, the scaling proposed by Wu *et al.* presents the same difficulty as Gillespie's, already pointed out before, concerning neutral projectiles, since it also goes to 0 for $q = 0$. Another important point in the case of the Wu scaling is that there are appreciable deviations between the results given by Eq. (13) and He ionization cross sections not only by neutral but, also, low-charged projectiles. In Fig. 5, the scaled ionization cross section $\sigma_{\rm ion}/q$ of He is plotted as a function of the scaled velocity $(v/q^{1/4})$ up to 1.5 a.u., for projectiles with charge states ranging from 0 to 30, namely, H^0 [53], He^0 and Ne^0 [54], He^+ [55], He^{2+} and Li^{3+} [3], C^0, C^+, C^{2+}, N^0, N^+, N^{2+}, N^{3+}, O^0, and O^+ [48], $I^{5+\,\rm to\,16+}$ [8], and Ar^{16+} and Xe^{30+} [7].

Two main deviations from the Wu scaling can be seen in this figure, which describes the data for highly charged and bare projectiles quite well for velocities between 0.7 and 1.5 a.u. For scaled velocities below $\approx$0.7 a.u., the Ar^{16+} and Xe^{30+} data from [7] tend to lie above the scaled cross-section curve, a fact that is discussed by those authors in detail. But, the scaled cross sections for low-charged dressed projectiles seem to be quite velocity independent, lying along a plateau which can be one order of magnitude higher than the scaled curve, even in the velocity region where Eq. (12) provides a good description of the bare- or highly-charged-ion data.

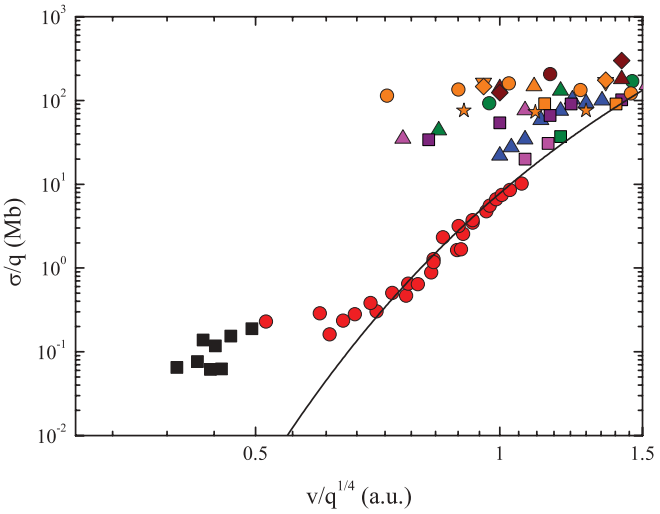

FIG. 5. (Color online) Scaled ionization cross sections ($\sigma_{\rm ion}$/q) of He by several projectiles as a function of the scaled velocity ($v/q^{1/4}$). Experiment: orange squares, H^0 [53]; orange up triangles, C^0; orange down triangles, N^0; orange diamonds, O^0, all from [48]; orange circles, He^0, and orange stars, Ne^0, both from [54]; purple squares, He^+ [55]; purple circles, C^+; purple triangles, N^+; and purple diamonds, O^+, all from [48]; green squares, He^{2+} [3]; green circles, C^{2+}; green triangles, N^{2+}, both from [48]; magenta squares, Li^{3+} [3]; magenta triangles, N^{3+} [48]; blue triangles, $I^{5+\,\text{to}\,16+}$ [8]; red circles, Ar^{16+} and black squares, Xe^{30+}, both from [7]. The solid line is the scaling function given by Eq. (12).

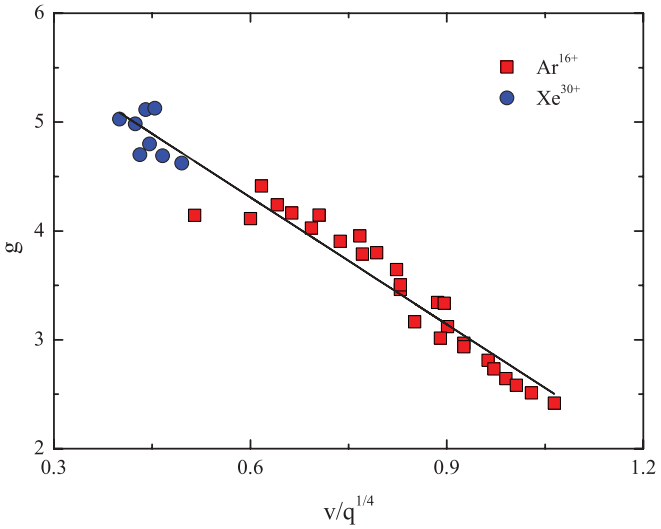

FIG. 6. (Color online) $g(v,q)$, given by Eq. (16) as a function of the scaled velocity ($v/q^{1/4}$). Experiment: red squares, Ar^{16+}, and blue circles, Xe^{30+}, both from [7]. The solid line is the linear fit given by Eq. (17) (see text).

It should be noted at this point that the scaling proposed in [13] shows quite good agreement with the Wu scaling for bare- and highly-charged-ion impact but, even if effective charges are used, it does not work for neutral and partially stripped projectiles, where it presents a similar behavior as that of Wu's as discussed above.

This nonunivocal behavior of the scaling function proposed by Wu *et al.* [7]—that is, the fact that these two groups of data present different velocity dependencies for the same velocity range—seems to indicate that there are two different mechanisms which contribute to the target ionization process.

First, let us consider the highly charged, low-velocity Ar^{16+} and Xe^{30+} data on He of Wu *et al.* [7] and assume that the scaled total ionization cross section $\sigma_{\rm ion}$ can be written in the same form as has been done for the Gillespie scaling [Eq. (5)], namely,

$$\sigma_{\rm ion} = q_{\rm W}^2 \sigma_{\rm p}, \tag{14}$$

where $q_{\rm W}$ is written as

$$q_{\rm W} = q e^{-g(v,q)}. \tag{15}$$

The function $g(v,q)$ describes the dependence of the scaled cross section on the projectile velocity and charge state in the low-energy regime for the ionization cross sections of He by highly charged, low-velocity projectiles. From Eqs. (14) and (15), this function can be written as

$$g(v,q) = -\frac{1}{2}\ln\left(\frac{\sigma_{\rm ion}/\sigma_{\rm p}}{q^2}\right). \tag{16}$$

A plot of $g(v,q)$ as a function of the scaled velocity proposed by Wu *et al.*, $(v/q^{1/4})$, is shown in Fig. 6, where $\sigma_{\rm ion}$ are the ionization cross sections of He by the highly charged, low-velocity Ar^{16+} and Xe^{30+} projectiles of Wu *et al.* [7]. It can be seen that these highly charged data present an approximately linear behavior with the scaled velocity, represented here by

$$g_{\rm lin}(v,q) = A_0 + B_0\left(\frac{v}{q^{1/4}}\right), \tag{17}$$

with $A_0 = 6.3$ and $B_0 = -3.5$ for v in atomic units.

In the intermediate- to low-velocity regime, there are two competitive collision channels, namely, ionization and capture, whose dominance depends on the region of the target where the collision occurs.

For the capture process, there are two radii, which appear in the Bohr-Lindhard model for capture [56–58]: the capture radius, defined as

$$r_{\rm cap} = \frac{2q}{v^2}, \tag{18}$$

and the release radius, defined as

$$r_{\rm rel} = \sqrt{\frac{qa}{I_{nl}}} = \frac{\sqrt{q}}{(I_{nl})^{3/4}}, \tag{19}$$

where a is the target electron orbital radius in atomic units.

It has been observed that the parameter which provides a clearer separation between the two distinct groups of the low-energy data shown in Fig. 5 is the ratio between the release and the adiabatic radii,

$$R = \frac{r_{\rm rel}}{r_{\rm adiab}} = \frac{\sqrt{q}}{2\gamma v}(I_{nl})^{1/4}. \tag{20}$$

In Fig. 7, the ratio between g, given by Eq. (16), and the linear function $g_{\rm lin}$, given by Eq. (17), of all the low-energy data of Fig. 5 is plotted as a function of the ratio R. It can be seen that the separation between the two groups of data occurs for $R \simeq 2.0$. While the ratios $g/g_{\rm lin}$ for the Ar^{16+} and Xe^{30+} data of [7] lie of course around 1, the ratios for the other,

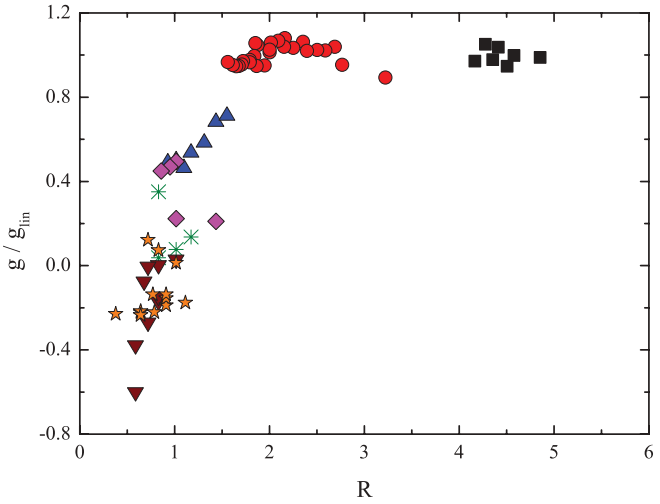

FIG. 7. (Color online) Ratio $g / g_{\rm lin}$ as a function of the $R = r_{\rm rel}/r_{\rm adiab}$. Experiment: orange stars, $q = 0$ [48,53,54]; brown down triangles, $q = 1$ [48,55]; green asterisks, $q = 2$ [3,48]; magenta diamonds, $q = 3$ [3,48]; blue triangles, $q = 5 - 16$ [8]; red circles, $q = 16$; and black squares, $q = 30$, both from [7].

low-charge, projectiles are much lower, being around zero, but with a much larger dispersion. The low-velocity bare-ion He^{2+} and Li^{3+} data from [3], and highly charged $I^{5+\,\text{to}\,16+}$ data from [8] seem to bridge these groups.

For the low-energy He data, the capture radius is always larger than the release and adiabatic radii; these differences can be very large for highly charged projectiles. This reflects the fact that the capture is the dominant process, mainly for highly charged projectiles, in which case almost all released electrons are captured and ionization is due to essentially a kind of "unsuccessful capture." The fact that this group only appears for values of $r_{\rm rel} \gtrsim 2.0 r_{\rm adiab}$ indicates that these released, but not-captured, electrons open a new channel for ionization, in which the electrons are not ejected due to a "direct impact" with the projectile, but rather due to an unsuccessful capture. However, when the projectile charge decreases, capture—although still the dominant process—becomes less important, and the capture radius is of the same order of the release and the adiabatic radii.

Moreover, Fig. 7 also shows that the parameter R provides the means for a univocal description of the low-energy ionization cross sections of the He atom. Thus, it is here proposed to consider the charge q, which appears in Eqs. (6) and (15), as a function of the ratio R, rather than as a function of q and v in the form

$$q(R) = q + \frac{q_{\rm scr} - q}{e^{(R-R_0)/\alpha(q)} + 1}, \tag{21}$$

where q is the projectile charge state, $q_{\rm scr}$ is the screened projectile charge given by Eq. (10), $\alpha(q) = \alpha_0 q^{1/4}$, where α_0 is an adjustable parameter, here taken as 0.01 in all cases, and R_0 is the value of the ratio R for which the transition between the two different ionization regimes occurs. It was found that $R_0 = 2.5$ provided the best overall fit to the data. This function $q(R)$, inspired in the Fermi-Dirac distribution law, provides a smooth connection between those two different ionization regimes, instead of using a step function. It tends to q for $R \gg R_0$ (corresponding to highly charged slow projectiles, for which ionization is dominated by the unsuccessful capture mechanism) and to $q_{\rm scr}$ for $R \ll R_0$ (low-charged fast projectiles, for which ionization is dominated by the direct impact mechanism).

D. Connection of the low-, intermediate-, and high-velocity regimes for the He target

If one wishes to extend this procedure to faster collisions, one should consider that, as mentioned before, for higher velocities, the scaling proposed by Gillespie provides a good description of the ionization of H—and, to a lesser extent, of He —atoms by highly charged projectiles [14,16]. So, here we propose a scaling for the ionization cross section of He—to be extended in the next section to other atomic and molecular targets whose outermost electrons occupy np subshells—which attempts to overcome the limitations of the Gillespie, Wu, and other scalings, concerning neutral projectiles and covering a wide range of projectile velocities.

In the proposed scaling the scaled total ionization cross section $\sigma_{\rm ion}$ is still calculated in a way similar to those given by Eqs. (5) and (14), that is,

$$\sigma_{\rm ion} = q_{\rm eff}^2 \sigma_{\rm p}, \tag{22}$$

where the parameter $q_{\rm eff}$ is defined as

$$q_{\rm eff} = q(R) e^{-h}, \tag{23}$$

with the new function $h(v,q,q_{\rm scr},R)$ given by

$$h(v,q,q_{\rm scr},R) = g(v,q) + \frac{f(v,q_{\rm scr}) - g(v,q)}{e^{(R-R_0)/\alpha(q)} + 1}, \tag{24}$$

where $f(v,q_{\rm scr})$ is the "modified Gillespie" scaling, given by Eq. (8), and $g(v,q)$ is the linear function, given by Eq. (17), and which is based on the Wu scaling.

This function $h(v,q,q_{\rm scr},R)$, which has been constructed using the same procedure of $q(R)$, shows a similar behavior with the ratio R. For large values of R when compared to R_0, the function h is essentially given by the linear function $g(v,q)$, which depends on the projectile charge state q, and refers to highly charged slow projectiles. On the other hand, when $R \ll R_0$, which are related essentially to high-velocity collisions, the function h is given by the modified Gillespie scaling $f(v,q_{\rm scr})$, and is a function of the effective charge rather than the actual charge state of the projectile.

The results of the proposed scaling for the total ionization of He targets by different projectiles, ranging from neutrals to highly stripped ones, are shown in Fig. 8. In this figure the scaled experimental ionization cross sections $\sigma_{\rm ion}^{\rm expt} / q_{\rm eff}^2$, where $\sigma_{\rm ion}^{\rm expt}$ is the experimental total ionization cross section and $q_{\rm eff}$ is given by Eq. (23), are plotted as a function of the square of the collision velocity, for the following projectiles: H^0 from [48,53], He^0 from [48,54], H^+, He^{2+}, and Li^{3+} all from [3], Ar^{16+} and Xe^{30+} from [7], and $I^{5+\,\text{to}\,16+}$ from [8]. The curve represents the scaled ionization cross sections for singly charged projectiles $\sigma_{\rm p}$, given by Eq. (3).

Although providing a reasonable fit for some of the experimental data, mainly in the high-velocity regime, the proposed scaling fails to describe the experimental results in the intermediate- to low-velocity region, mainly those related

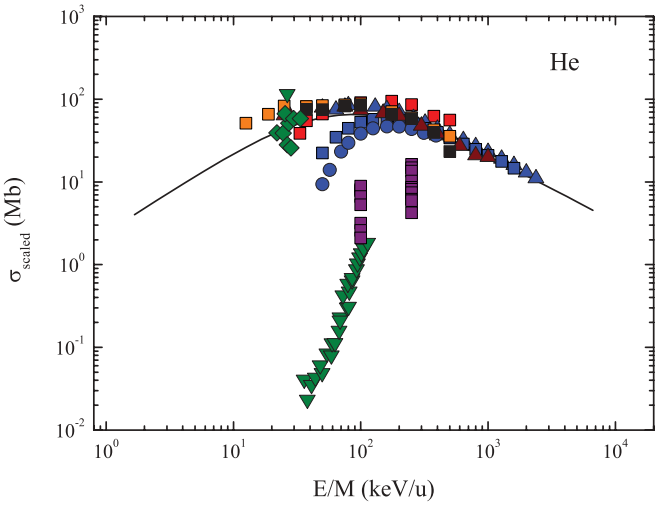

FIG. 8. (Color online) Scaled experimental ionization cross sections ($\sigma_{ion}^{exp}/q_{eff}^2$) of He by several projectiles as a function of E/M. Experiment: black up triangles, H^0 [48]; brown up triangles, H^0 [53]; blue up triangles, H^+ [3]; black squares, He^0 [48]; orange squares, He^0 [54]; red squares, He^+ [55]; blue squares, He^{2+} [3]; blue circles, Li^{3+} [3]; purple squares, $I^{5+\,to\,16+}$ [8]; and green inverted triangles, Ar^{16+} and green diamonds, Xe^{30+}, both from [7]. The solid line is the scaled ionization cross sections for singly charged projectiles σ_p given by Eq. (3).

to highly charged projectiles, such as Ar^{16+}, Xe^{30+}, and $I^{5+\,to\,16+}$. These discrepancies could not be eliminated—or even reduced to a reasonable level—by varying the fitting parameters β and λ, in the function $f(v,q_{eff})$, and α_0, in the functions $q(R)$ and $h(v,q,q_{eff},R)$. The physical reason for these discrepancies will be discussed in the next section.

E. Inclusion of the binding correction

During the 1970s, Brandt and co-workers presented a series of articles in which they introduced several corrections to first-order and semiclassical treatments of inner-shell ionization by charged projectiles [59–66]. One of the most important of these corrections refers to the increase of the binding energy of the target active electron due to the Coulomb field of the impinging projectile with a corresponding decrease of the ionization cross section [51,59–63,67].

In general, using hydrogenic wave functions to describe the active target electrons, the binding energy of an electron with principal quantum number n can be written in atomic units as

$$I = \frac{(Z_T^*)^2}{n^2}, \tag{25}$$

where $Z_T^* = Z_T - s$ is the screened target atomic number, with Z_T being the target atomic number and s the Slater screening constant [68]. In the case of the atomic targets considered here, the values of Z_T^* for the outermost electrons were 1.7, 5.85, and 6.75 for He, Ne, and Ar, respectively. The values of Z_T^* for molecules were calculated under the assumption that only the nonbonding electrons contribute to the screening; that is, the electrons participating in the covalent bonding do not provide any screening. For example, for water one has $Z_T^* = 8 - 2 \times 0.85 - 3 \times 0.35 = 5.25$, and, for uracil, $Z_T^* = 6 - 2 \times 0.85 - 0 \times 0.35 = 4.3$.

The binding correction consists essentially in considering that, during the collision, the active target electrons are subject to the combined Coulomb field of the projectile and the target, so that their ionization energies are rewritten as

$$I^* = \frac{(Z^*)^2}{n^2} = \left(\frac{Z^*}{Z_T^*}\right)^2 I = \epsilon I, \tag{26}$$

where Z^*, given by

$$Z^* = Z_P^* + Z_T^*, \tag{27}$$

is the total effective nuclear charge due to the presence of the projectile, whose charge is represented by Z_P^*, near the distance of closest approach, considering that the wave function of the active target electron evolves adiabatically during the transition. Thus, ϵ represents the correction factor for the ionization energy of the active electron due to the binding effect which can be written as

$$\epsilon = \left(\frac{Z^*}{Z_T^*}\right)^2 = \left(1 + \frac{Z_P^*}{Z_T^*}\right)^2. \tag{28}$$

The parameter Z_P^* has been introduced by several authors by means of different functions of the collision velocity, also depending on the atomic subshell of the active electron (see, for instance, Refs. [51,59–61,63]). Here, aiming to provide the simplest description possible for the binding correction, we have written this parameter as

$$Z_P^* = \kappa(q-1)e^{-r_{adiab}}. \tag{29}$$

As will be seen, the parameter κ will be taken as 0.6 for hydrogen and 1.0 for all the other targets considered here. Thus, the binding correction factor can be written as

$$\epsilon = \left[1 + \kappa\frac{(q-1)}{Z_T^*}e^{-r_{adiab}}\right]^2. \tag{30}$$

The increase in the binding energies of the target active electrons occurs only for the direct ionization process; that is, for $R \leqslant R_0$. So, following the reasoning used above to perform the smooth connection between the two different ionization regimes, one can define an effective binding correction factor as

$$\bar{\epsilon} = 1 + \frac{\epsilon - 1}{e^{(R-R_0)/\alpha(q)} + 1}. \tag{31}$$

We can define a scaled experimental ionization cross section as

$$\sigma_{scaled}^{exp}(E/M\bar{\epsilon}) = \frac{\bar{\epsilon}^2\sigma_{ion}^{exp}(E/M\bar{\epsilon})}{q_{eff}^2} = \sigma_P(E/M), \tag{32}$$

with q_{eff} and $\bar{\epsilon}$ given by Eqs. (23) and (31), respectively.

In Eq. (32), the scaled ionization cross section for protons σ_P is calculated as a function of E/M because, from Eq. (30), $\epsilon = 1$ for protons. It should be remarked that, since the parameters used to calculate the scaled ionization cross section for protons σ_P have been obtained empirically, the binding effect is already included in the fitting given by Eqs. (3) and (4). The parameter $\bar{\epsilon}$ provides an additional correction, due to the binding effect

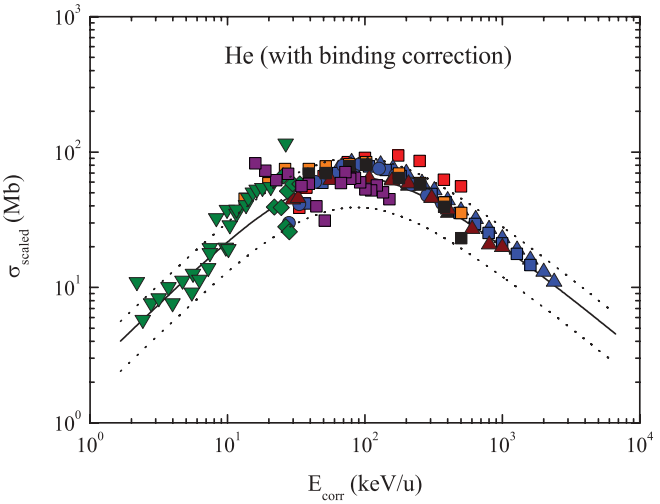

FIG. 9. (Color online) Scaled experimental ionization cross sections including the binding correction $\sigma_{\rm ion}^{\rm exp}\bar{\epsilon}^2/q_{\rm eff}^2$ of He by several projectiles as a function of $E_{\rm corr} = E/(M\bar{\epsilon})$ (see text). The experimental data are the same as in Fig. 8. The solid line is the scaled ionization cross sections for singly charged projectiles $\sigma_{\rm p}$ given by Eq. (3) and the dotted lines represent a deviation of ±40% of the solid line (see text).

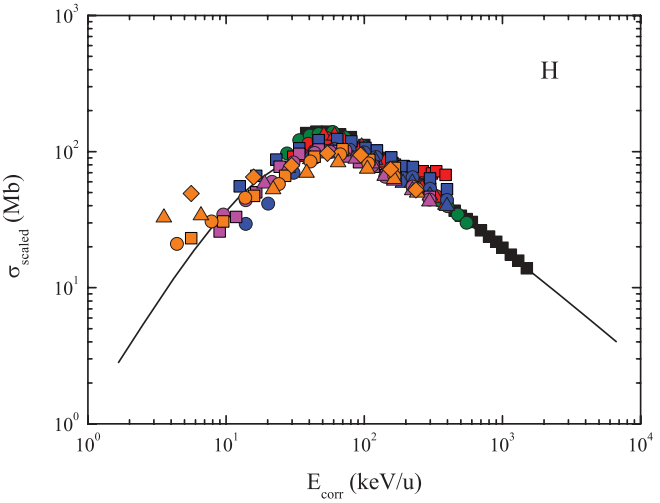

FIG. 10. (Color online) The same as in Fig. 8 for the H target. Experiment: black squares, H^+ and green circles, He^{2+}, both from [28]; red squares, Li^+; red circles, Li^{2+}; and red triangles, Li^{3+}, all from [69]; blue squares, C^{2+}; blue circles, C^{3+}; blue triangles, C^{4+}; magenta squares, O^{2+}; magenta circles, O^{3+}; and magenta triangles, C^{4+}, all from [70]; orange squares, Ar^{3+}; orange circles, Ar^{4+}; orange triangles, Ar^{5+}; and orange diamonds, Ar^{6+}, all from [71].

for other projectiles, which act on top of the one for protons. Thus, the ionization cross section is obtained as

$$\sigma_{\rm ion} = \frac{q_{\rm eff}^2}{\bar{\epsilon}^2}\sigma_{\rm P}(E/M\bar{\epsilon}). \tag{33}$$

The results of the proposed scaling for the total ionization of He considering the binding correction are shown in Fig. 9, where the scaled experimental ionization cross section, $\sigma_{\rm scaled}^{\rm exp}$, given by Eq. (32), is plotted as a function of the square of the collision velocity, including the binding correction $E_{\rm corr} = E/(M\bar{\epsilon})$, for the same collision systems as those of Fig. 8. The curve represents the scaled ionization cross sections for singly charged projectiles $\sigma_{\rm p}$ given by Eq. (3), also with I_{nl} multiplied by $\bar{\epsilon}$.

It can be readily seen that the introduction of the binding correction factor produces an appreciable improvement in the scaling, which can now be considered to be very good, within a deviation of ±40%, represented by the dotted lines, mainly if one takes into account the very broad range of collision velocities and projectile charge states.

IV. PROJECTILE SCALING FOR OTHER ATOMIC AND MOLECULAR TARGETS

The results of the proposed scaling for the total ionization of H, Ne, Ar, water, and uracil targets by different projectiles, ranging from neutrals to highly stripped ones, are shown in Figs. 10–14. The solid lines in these figures are the scaled ionization cross sections for protons $\sigma_{\rm p}$ obtained as the sum of the scaled cross sections calculated for each orbital nl using Eq. (3). As in Sec. II, the ionization energies of the outer-shell electrons of the noble gases were taken from [36], while those of the valence molecular orbitals of the water and uracil targets were those presented by Hwang *et al.* [37] and Holland *et al.* [38], respectively. The values of δ_{nl}, I_{nl}, and Z_{nl} for the nl orbitals considered here for these targets are summarized in Table II.

The fitting parameters for all these scalings, including that for He presented in the preceding section, are summarized in Table III. It should be noted that the values of the parameter B, which appear in Eq. (4), for H and Ne differ from those for the other targets, in order to obtain better fits for the proton data of Refs. [28] and [4], respectively. In the Appendix, a sample calculation is presented with the aim of helping the reader to follow all the steps to obtain the scaled ionization cross sections which are proposed here.

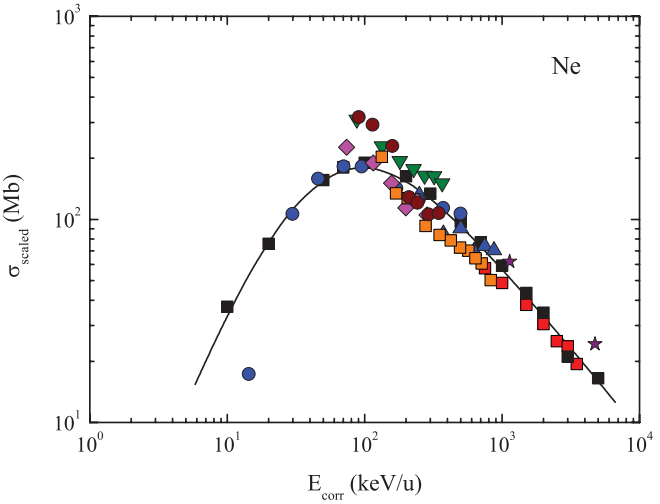

FIG. 11. (Color online) The same as in Fig. 8 for the Ne target. Experiment: black squares, H^+ [4]; red squares, H^+ [72]; blue up triangles, He^+ [43]; blue circles, He^{2+} [19]; orange squares, Li^{3+} [73]; green inverted triangles, B^{2+} [74]; magenta diamonds, C^{3+} [75]; brown circles, Ne^{3+} [76]; and purple stars, C^{6+} [11].

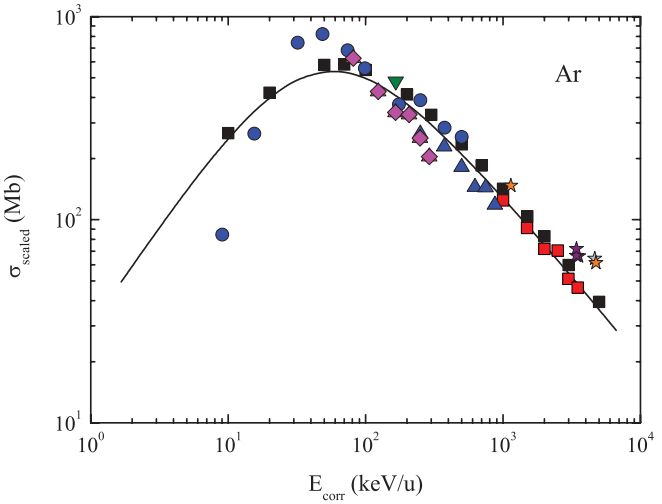

FIG. 12. (Color online) The same as in Fig. 8 for the Ar target. Experiment: black squares, H^+ [4]; red squares, H^+ [72]; blue up triangles, He^+ [43]; blue circles, He^{2+} [19]; orange up triangles, C^{3+} [45]; magenta diamonds, C^{3+} [46]; green inverted triangles, $Ar^{4+\text{ to }14+}$ [47]; orange stars, C^{6+}; purple stars, $Nb^{23+,31+,34+}$; and gray stars, Pb^{54+}, all from Ref. [11].

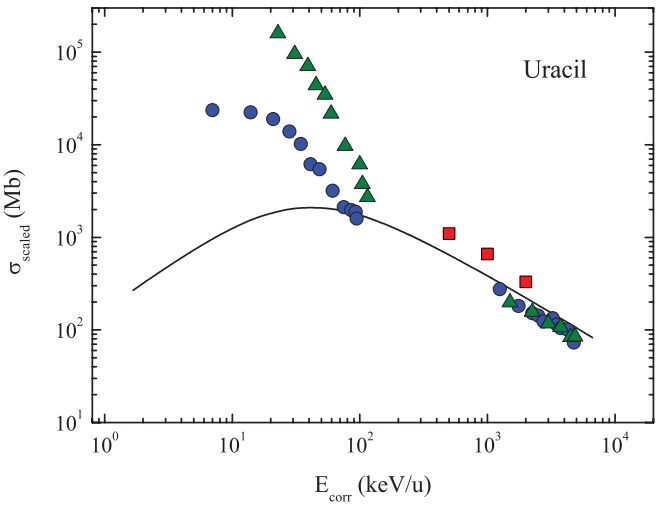

FIG. 14. (Color online) The same as in Fig. 8 for the uracil target. Experiment: red squares, H^+ from Iriki *et al.* as cited by Galassi *et al.* [35]; blue circles, C^{4+} [82]; and green triangles, O^{6+} [82].

These figures show that the proposed scaling describes quite well the ionization cross sections for the atomic and molecular targets, with the exception of the intermediate- to low-velocity data of the ionization of uracil by C^{4+} and O^{6+} projectiles reported by Agnihotri *et al.* [82], where the deviations from the scaled ionization cross sections for protons are very large, not only in absolute values but also in trend (see Fig. 14). These deviations begin around 100 keV/u and increase as the collision velocity decreases. The explanation for these discrepancies is that the experimental data reported by Agnihotri *et al.* do not discriminate between the ionization and transfer-ionization (TI) processes. Since electron capture (including TI) is the dominant process in collisions with low-velocity highly charged projectiles, it is not surprising that the experimental cross sections present such a different behavior than the proposed scaling.

The contribution of TI can be included in an approximate way if the semiclassical Bohr-Lindhard model as presented by Knudsen *et al.* [57], normalized to the lowest-energy data of Agnihotri *et al.*, is added to the ionization calculations using the proposed scaling. Although this model is for total electron capture, i.e., single electron capture plus TI, it should give a fair description for the TI energy dependence. This is shown in Fig. 15 for C^{4+} projectiles. It can be seen that the sum of the TI and the ionization cross sections provides a good description of the experimental data for the entire energy range.

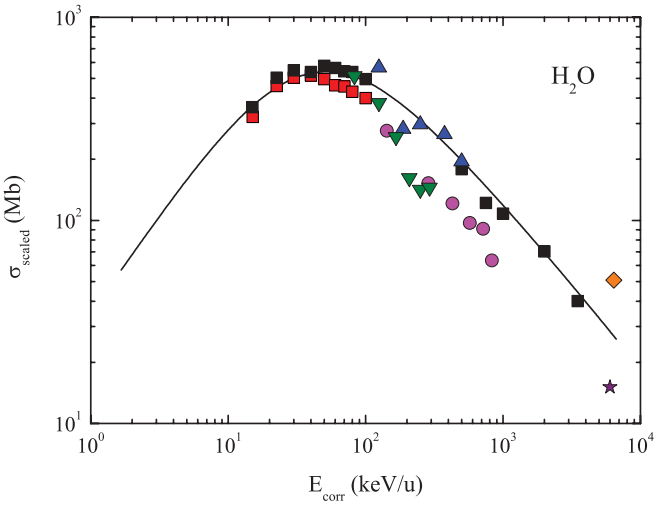

FIG. 13. (Color online) The same as in Fig. 8 for the water target. Experiment: red squares, H^0 and black squares, H^+ [33]; blue up triangles, He^+ [77]; magenta circles, Li^{3+} [78]; green inverted triangles, C^{3+} [79]; purple stars, C^{6+} [80]; and orange diamonds, Xe^{44+} [81].

TABLE II. Parameters δ_{nl}, Z_{nl}, and I_{nl} (a.u.) for the nl orbitals of the H, Ne, Ar, water, and uracil targets.

Target	Orbital	δ_{nl}	Z_{nl}	I_{nl}
H	$1s$	0.66	1	1.00
He	$1s$	0.80	2	1.81
Ne	$2p$	0.55	6	1.70
	$2s$	0.60	2	3.86
Ar	$3p$	0.55	6	1.18
	$3s$	0.6	2	2.56
	$2p$	0.55	6	19.1
	$2s$	0.6	2	24.6
H_2O	$1b_1$	1.00	2	0.93
	$3a_1$	0.66	2	1.14
	$1b_2$	0.66	2	1.46
	$2a_1$	0.66	2	2.71
Uracil	$5a''$; $4a''$; $16a''$; $15a'$	0.50	8	0.75
	$3a''$; $2a''$; $14a'$; $13a'$	0.50	8	1.01
	$12a'$; $1a''$; $11a'$	0.50	6	1.13

TABLE III. Parameters used in the scaled ionization cross sections, given by Eq. (32), of atomic and molecular targets by various projectiles.

	Related quantity	Equations	All targets	H	He	Ne	Ar	H_2O	Uracil
A	$F(x)$	(4)	6150						
B	$F(x)$	(4)		0.11	0.07	0.11	0.07	0.07	0.07
C	$F(x)$	(4)	0.014						
A_0	$g(v,q)$	(17)	6.3						
B_0	$g(v,q)$	(17)	−3.5						
R_0	r_{rel}/r_{adiab}	(21), (24), (31)	2.5						
λ	$f(v,q)$	(7), (8), (24)		0.06	0.06	0.50	0.80	1.10	0.60
γ	r_{adib}	(11)		1.0	0.82	0.85	1.0	1.4	1.4
κ	Z_P^*	(29)		0.6	1.0	1.0	1.0	1.0	1.0
$(q_{asym})_H$	q_{eff}	See text		0.60	0.65	0.60	0.80		
$(q_{asym})_{He}$	q_{eff}	See text		0.90	0.90	0.90	0.90		
α_0	$\alpha(q)$	(21), (24), (31)	0.01						

As a last point, it is instructive to analyze the behavior of the effective charge q_{eff} given by Eq. (33) as

$$q_{eff} = \bar{\epsilon}\sqrt{\frac{\sigma_{ion}^{exp}(E/M)}{\sigma_P(E/M\bar{\epsilon})}} \tag{34}$$

as a function of the collision energy. In Fig. 16, the values of q_{eff} are plotted as a function of the square of the velocity for collisions of C^{3+} projectiles on Ne. The line represents the calculated values from Eq. (23), while the squares were obtained from Eq. (34), for the experimental values of Kirchner *et al.* [75]. For high velocities, the values of q_{eff} tend to q, as expected. As the collision velocity decreases, the effect of the saturation of the ionization probabilities becomes important, as described by the Gillespie-type scaling [see, for instance, Eqs. (5)–(8)], and q_{eff} decreases, so that unitarity of the ionization probability is preserved. For even smaller velocities, this behavior is reversed and q_{eff} increases again, in this instance due to the decrease of the screening of the projectile nuclear charge by its electrons as the velocity decreases, as discussed in Sec. III B. This behavior is different than that observed in the energy loss of ions and atoms traversing matter [83–85], because, in the latter, the charge of the projectile varies continuously during the penetration process, while the effective charge shown in Fig. 16 has been obtained for a fixed value of q for the whole velocity range, thus representing a completely different physical situation.

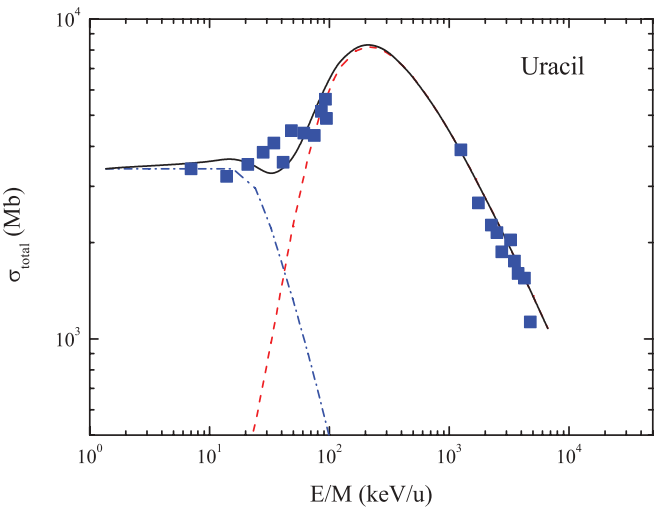

FIG. 15. (Color online) Total positive ion production for collisions of C^{4+} projectiles and the uracil target. Experiment: blue squares, [82]. Theory: red dashed line, ionization cross sections using the present scaling, Eq. (32); blue dash-dotted line, capture cross sections using the Bohr-Lindhard model [57]; and full line, sum of the ionization and capture cross sections.

V. SUMMARY AND CONCLUSIONS

A scaling for the total ionization cross sections of atomic and molecular targets by neutral to highly charged projectiles with energies ranging from a few keV/u to many MeV/u has been proposed. This scaling describes quite well the existent experimental data for collision systems as diverse as H^+ on H, Xe^{30+} on He, or O^{6+} on uracil.

The reason for developing this scaling is that simple scalings, such as Bohr's, Olson's, or the one presented in [13], try to write the ratio between the ionization cross section and some power of the projectile charge state q as a single function

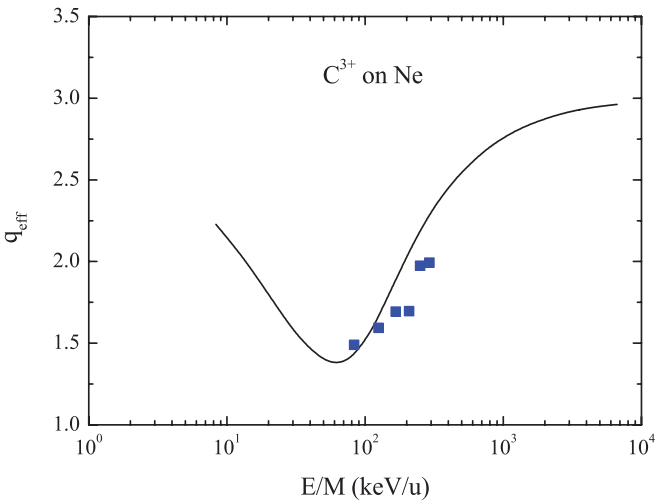

FIG. 16. (Color online) Projectile effective charge as a function of E/M in keV/u for collisions of C^{3+} projectiles on Ne. The black line is the value of q_{eff} obtained using Eq. (23). Experiment: blue squares, q_{eff} obtained from Eq. (34) for the data of Ref. [75].

of the ratio of the collision velocity by another power of q, which renders them, on the one hand, very easy to use but, on the other hand, too limited, both from the mathematical and physical points of view, because they cannot take into account either other processes which compete with ionization at low collision energies, or cover a wide range of projectile charge states, for a large variety of targets.

The scaling presented here has been obtained using the following strategy. First, a target scaling for protons was developed as a function of the collision velocity. Then, this target scaling was left intact, except for the introduction of the effect of the projectile on the binding energy of the active target electrons, and all the physical aspects concerning how the projectile affects the target ionization dynamics have been included by means of an effective charge $q_{\rm eff}$, which is a function of the projectile charge state as well as its velocity. The scaled cross section was, then, obtained as a product of the square of the effective charge by the scaling function for protons.

The usefulness and adequacy of the line of reasoning of the proposed scaling lie on two main features. First, it has few free parameters, which are all velocity independent and whose values, with one exception, do not vary appreciably for the projectiles and atomic and molecular targets considered here. The only exception is the parameter λ, which is related to the high-velocity behavior of the cross section, described by the scaling introduced by Gillespie [14], whose values for the H and He targets are one order of magnitude smaller that those for the other targets.

The second important feature is that the proposed scaling has been built considering the characteristics of the collision systems, taking into account the various physical processes that lead to target ionization and the velocity regions where each of them dominates, and trying to perform a smooth transition between them.

It should be emphasized that the parameters chosen here are not necessarily those that will provide the best possible fit for a specific projectile-target system, but rather they are intended to act as guiding values for estimating ionization cross sections for systems where experimental data are scarce or nonexistent. As new experimental data become available, the values of these parameters can be further refined in order to provide even better descriptions of the ionization cross sections. This is the case, for instance, of the parameter λ, whose values for targets so different as Ne, Ar, water, and uracil lie between 0.55 and 1.1, so that one can assume that, for other atoms and molecules, its value will probably also be within this range.

ACKNOWLEDGMENTS

This work was supported in part by the Brazilian agencies CNPq, FAPERJ, and MCT(PRONEX).

TABLE IV. Sample calculation of the scaled ionization cross section for 100 keV/u C^{3+} on Ne.

Quantity or parameter	Equation or definition	Value
v	$0.2\sqrt{E/M\ (\mathrm{keV/u})}$	2.00
γ	Table III	0.85
$r_{\rm adiab}$	Eq. (11)	2.00
$q_{\rm scr}$	Eq. (10)	3.51
β	Eq. (9)	0.413
λ	Table III	0.50
$f(v,q_{\rm scr})$	Eq. (8)	0.840
$v/q^{1/4}$		1.52
$g(v,q)$	Eq. (17)	0.980
$r_{\rm rel}$	Eq. (19)	1.16
R	$r_{\rm rel}/r_{\rm adiab}$	0.580
$\alpha(q)$	$\alpha_0 q^{1/4}$	0.0132
$q(R)$	Eq. (21)	3.51
$h(v,q,q_{\rm scr},R)$	Eq. (24)	0.840
$q_{\rm eff}$	Eq. (23)	1.515
s	Ref. [68]	4.15
$Z_{\rm T}^*$	$Z_{\rm T}-s$	5.85
$Z_{\rm P}^*$	Eq. (29)	0.271
ϵ	Eq. (30)	1.095
$\bar{\epsilon}$	Eq. (31)	1.095
$E_{\rm corr}$	$E/(M\bar{\epsilon})$	91.3 keV/u
I_{2p}	Table II	1.70
δ_{2p}	Table II	0.55
Z_{2p}	Table II	6
x_{2p}	$E_{\rm corr}/I_{2p}$	53.7 keV/u
$F(x_{2p})$	Eq. (4)	149 Mb
$[\sigma_{\rm p}(E_{\rm corr})]_{2p}$	$F(x_{2p})Z_{2p}\delta_{2p}/I_{2p}^2$	170 Mb
I_{2s}	Table II	3.86
δ_{2s}	Table II	0.60
Z_{2s}	Table II	2
x_{2s}	$E_{\rm corr}/I_{2s}$	23.7 keV/u
$F(x_{2s})$	Eq. (4)	118 Mb
$[\sigma_{\rm p}(E_{\rm corr})]_{2s}$	$F(x_{2s})Z_{2s}\delta_{2s}/I_{2s}^2$	9.50 Mb
$\sigma_{\rm p}(E_{\rm corr})$	$[\sigma_{\rm p}(E_{\rm corr})]_{2p}+[\sigma_{\rm p}(E_{\rm corr})]_{2s}$	180 Mb
$\sigma_{\rm ion}(E/M=100\ \mathrm{keV/u})$	Eq. (33)	345 Mb

APPENDIX: SAMPLE CALCULATION OF THE SCALED CROSS SECTION

In Table IV we present a sample calculation of the scaled ionization cross section for 100 keV/u C^{3+} on Ne. This system has been chosen because it contains most of the different features of the proposed scaling, including the binding correction discussed in Sec. III E. The first column of Table IV lists the parameter or quantity, the second provides the equation which defines it in the text, while the last column shows the calculated value.

[1] N. Bohr, K. Dan. Vidensk. Selsk. Mat. Fys. Medd. **18**(8), (1948).
[2] H. Bethe, Ann. d. Physik **5**, 325 (1930).
[3] M. B. Shah and H. B. Gilbody, J. Phys. B **18**, 899 (1985).
[4] M. E. Rudd, Y.-K. Kim, D. H. Madison, and J. W. Gallagher, Rev. Mod. Phys. **57**, 965 (1985).
[5] O. Woitke, P. A. Závodszky, S. M. Ferguson, J. H. Houck, and J. A. Tanis, Phys. Rev. A **57**, 2692 (1998).

[6] H. Knudsen, L. H. Andersen, P. Hvelplund, G. Astner, H. Cederquist, H. Danared, L. Liljeby, and K.-G. Rensfeld, J. Phys. B **17**, 3545 (1984).

[7] W. Wu, C. L. Cocke, J. P. Giese, F. Melchert, M. L. A. Raphaelian, and M. Stöckli, Phys. Rev. Lett. **75**, 1054 (1995).

[8] S. Datz *et al.*, Phys. Rev. A **41**, 3559 (1990).

[9] R. E. Olson, Phys. Rev A **18**, 2464 (1978).

[10] R. E. Olson, K. H. Berkner, W. G. Graham, R. V. Pyle, A. S. Schlachter, and J. W. Stearns, Phys. Rev. Lett. **41**, 163 (1978).

[11] A. S. Schlachter, K. H. Berkner, W. G. Graham, R. V. Pyle, P. J. Schneider, K. R. Stalder, J. W. Stearns, J. A. Tanis, and R. E. Olson, Phys. Rev. A **23**, 2331 (1981).

[12] Clara Illescas, L. F. Errea, L. Méndez, B. Pons, I. Rabadán, and A. Riera, Phys. Rev. A **83**, 052704 (2011).

[13] R. D. DuBois, E. C. Montenegro, and G. M. Sigaud, in *Application of Accelerators in Research and Industry 2000*, edited by J. L. Duggan and I. L. Morgan, AIP Conf. Proc. No. X (to be published).

[14] G. H. Gillespie, J. Phys. B **15**, L729 (1982).

[15] W. Wu, E. F. Deveney, S. Datz, D. D. Desai, H. F. Krause, J. M. Sanders, C. R. Vane, C. L. Cocke, and J. P. Giese, Phys. Rev. A **53**, 2367 (1996).

[16] I. D. Kaganovich, E. Startsev, and R. C. Davidson, New J. Phys. **8**, 278 (2006).

[17] D. R. Bates and G. Griffing, Proc. Phys. Soc. A **68**, 90 (1955).

[18] R. D. DuBois, A. C. F. Santos, G. M. Sigaud, and E. C. Montenegro, Phys. Rev. A **84**, 022702 (2011).

[19] R. D. DuBois and S. T. Manson, Phys. Rev. A **35**, 2007 (1987).

[20] A. Brahme, Int. J. Radiat. Oncol. Biol. Phys. **58**, 603 (2004).

[21] E. C. Montenegro, A. C. F. Santos, and G. M. Sigaud, in *Application of Accelerators in Research and Industry 2000*, edited by J. L. Duggan and I. L. Morgan, AIP Conf. Proc. No. 576, (AIP, Melville, NY, 2001), p. 96.

[22] R. D. DuBois, L. H. Toburen, and M. E. Rudd, Phys. Rev. A **29**, 70 (1984).

[23] Y. K. Kim and M. E. Rudd, Phys. Rev. A **50**, 3954 (1994).

[24] E. G. Cavalcanti, G. M. Sigaud, E. C. Montenegro, and H. Schmidt-Böcking, J. Phys. B **36**, 3087 (2003).

[25] J. H. McGuire, *Electron Correlation Dynamics in Atomic Collisions* (Cambridge University Press, New York, 1997), Chap. 4.

[26] M. M. Sant'Anna, E. C. Montenegro, and J. H. McGuire, Phys. Rev. A **58**, 2148 (1998).

[27] N. F. Mott and H. S. W. Massey, *The Theory of Atomic Collisions* (Oxford University Press, London, 1965), p. 503.

[28] M. B. Shah and H. B. Gilbody, J. Phys. B **14**, 2361 (1981).

[29] M. E. Rudd, R. D. DuBois, L. H. Toburen, C. A. Ratcliffe, and T. V. Goffe, Phys. Rev. A **28**, 3244 (1983).

[30] N. V. Fedorenko, V. V. Afrosimov, R. N. Il'in, and E. S. Solovev, in *Proceedings of the Fourth International Conference on Ionization Phenomena in Gases*, edited by N. R. Nillson (North-Holland, Amsterdam), Vol. 1, p. 47 (1960).

[31] L. H. Toburen, Phys. Rev. A **9**, 2505 (1974).

[32] M. B. Shah and H. B. Gilbody, J. Phys. B **15**, 3441 (1982).

[33] H. Luna, A. L. F. de Barros, J. A. Wyer, S. W. J. Scully, J. Lecointre, P. M. Y. Garcia, G. M. Sigaud, A. C. F. Santos, V. Senthil, M. B. Shah, C. J. Latimer, and E. C. Montenegro, Phys. Rev. A **75**, 042711 (2007).

[34] H. Luna, E. G. Cavalcanti, J. Nickles, G. M. Sigaud, and E. C. Montenegro, J. Phys. B **36**, 4717 (2003).

[35] M. E. Galassi, C. Champion, P. F. Weck, R. D. Rivarola, O. Fojón, and J. Hanssen, Phys. Med. Biol. **57**, 2081 (2012).

[36] S. Fraga, J. Karwowski, and K. M. S. Saxena, *Handbook of Atomic Data* (Elsevier Scientific Publishing Company, Amsterdam, 1976).

[37] W. Hwang, Y.-K. Kim, and M. E. Rudd, J. Chem. Phys. **104**, 2956 (1996).

[38] D. M. P. Holland, A. W. Potts, L. Karlsson, I. L. Zaytseva, A. B. Trofimov, and J. Schirmer, Chem. Phys. **353**, 47 (2008).

[39] L. H. Andersen, P. Hvelplund, H. Knudsen, S. P. Møller, J. O. P. Pedersen, S. Tang-Petersen, E. Uggerhøj, K. Elsener, and E. Morenzoni, Phys. Rev. A **41**, 6536 (1990).

[40] P. Hvelplund, H. Knudsen, U. Mikkelsen, E. Morenzoni, S. P. Møller, E. Huggerhøj, and T. Worm, J. Phys. B **27**, 925 (1994).

[41] H. Knudsen *et al.*, Phys. Rev. Lett. **101**, 043201 (2008).

[42] K. Paludan, H. Bluhme, H. Knudsen, U. Mikkelsen, S. P. Møller, E. Huggerhøj, and E. Morenzoni, J. Phys. B **30**, 3951 (1997).

[43] A. C. F. Santos, W. S. Melo, M. M. Sant'Anna, G. M. Sigaud, and E. C. Montenegro, Phys. Rev. A **63**, 062717 (2001).

[44] R. D. DuBois, Phys. Rev. A **36**, 2585 (1987).

[45] A. C. F. Santos, G. M. Sigaud, W. S. Melo, M. M. Sant'Anna, and E. C. Montenegro, Phys. Rev. A **82**, 012704 (2010).

[46] M. Saito, Y. Haruyama, N. Hamamoto, K. Yoshida, A. Itoh, and N. Imanishi, J. Phys. B **28**, 5117 (1995).

[47] T. Tonuma, H. Kumagai, T. Matsuo, and H. Tawara, Phys. Rev. A **40**, 6238 (1989).

[48] R. D. DuBois and L. H. Toburen, Phys. Rev. A **38**, 3960 (1988).

[49] F. Alvarado, S. Bari, R. Hoekstra, and Th. Schlathölter, J. Chem. Phys. **127**, 034301 (2007).

[50] F. Salvat, J. D. Martinez, R. Mayol, and J. Parellada, Phys. Rev. A **36**, 467 (1987).

[51] E. C. Montenegro and G. M. Sigaud, J. Phys. B **18**, 299 (1985).

[52] E. C. Montenegro and W. E. Meyerhof, Phys. Rev. A **43**, 2289 (1991).

[53] R. D. DuBois and A. Köver, Phys. Rev. A **40**, 3605 (1989).

[54] J. M. Sanders, R. D. DuBois, S. T. Manson, S. Datz, E. F. Deveney, H. F. Krause, J. L. Shinpaugh, and C. R. Vane, Phys. Rev. A **76**, 062710 (2007).

[55] R. D. DuBois, Phys. Rev. A **39**, 4440 (1989).

[56] N. Bohr and J. Lindhard, K. Dan. Vidensk. Selsk. Mat. Fys. Medd. **28**(7), (1954).

[57] H. Knudsen, H. K. Haugen, and P. Hvelplund, Phys. Rev. A **23**, 597 (1981).

[58] B. W. Ding, Phys. Scr. **85**, 015302 (2012).

[59] W. E. Brandt, R. Laubert, and I. Sellin, Phys. Rev. **151**, 56 (1966).

[60] G. Basbas, W. E. Brandt, and R. Laubert, Phys. Lett. A **34**, 277 (1971)

[61] G. Basbas, W. E. Brandt, and R. Laubert, Phys. Rev. A **7**, 983 (1973).

[62] G. Basbas, W. E. Brandt, and R. H. Ritchie, Phys. Rev. A **7**, 1971 (1973).

[63] W. E. Brandt and G. Lapicki, Phys. Rev. A **10**, 474 (1974).

[64] G. Basbas, W. E. Brandt, and R. Laubert, Phys. Rev. A **17**, 1655 (1978).

[65] W. E. Brandt and G. Lapicki, Phys. Rev. A **20**, 465 (1979).

[66] G. Lapicki, R. Laubert, and W. E. Brandt, Phys. Rev. A **22**, 1889 (1980).

[67] X.-Y. Xu, E. C. Montenegro, R. Anholt, K. Danzmann, W. E. Meyerhof, A. S. Schlachter, B. S. Rude, and R. J. McDonald, Phys. Rev. A **38**, 1848 (1988).

[68] J. C. Slater, Phys. Rev. **36**, 57 (1930).
[69] M. B. Shah and H. B. Gilbody, J. Phys. B **15**, 413 (1982).
[70] M. B. Shah and H. B. Gilbody, J. Phys. B **14**, 2831 (1981).
[71] M. B. Shah and H. B. Gilbody, J. Phys. B **16**, 4395 (1983).
[72] E. G. Cavalcanti, G. M. Sigaud, E. C. Montenegro, M. M. Sant'Anna, and H. Schmidt-Böcking, J. Phys. B **35**, 3937 (2002).
[73] I. Junger de Souza, H. Luna, W. Wolff, and E. C. Montenegro (unpublished).
[74] W. Wolff, H. Luna, A. C. F. Santos, E. C. Montenegro, and G. M. Sigaud, Phys. Rev. A **80**, 032703 (2009).
[75] T. Kirchner, A. C. F. Santos, H. Luna, M. M. Sant'Anna, W. S. Melo, G. M. Sigaud, and E. C. Montenegro, Phys. Rev. A **72**, 012707 (2005).
[76] J. Ullrich, K. Bethge, S. Kelbch, W. Schadt, H. Schmidt-Böcking, and K. E. Stiebing, J. Phys. B **19**, 437 (1986).
[77] P. M. Y. Garcia, G. M. Sigaud, H. Luna, A. C. F. Santos, E. C. Montenegro, and M. B. Shah, Phys. Rev. A **77**, 052708 (2008).
[78] A. C. Tavares, W. Wolff, H. Luna, and E. C. Montenegro (unpublished).
[79] H. Luna and E. C. Montenegro, Phys. Rev. Lett. **94**, 043201 (2005).
[80] C. Dal Cappello, C. Champion, O. Boudrioua, H. Lekadir, Y. Sato, and D. Ohsawa, Nucl. Instrum. Methods Phys. Res. B **267**, 781 (2009).
[81] G. H. Olivera, C. Caraby, P. Jardin, A. Cassimi, L. Adoui, and B. Gervais, Phys. Med. Biol. **43**, 2347 (1998).
[82] A. N. Agnihotri, S. Kasthurirangan, S. Nandi, A. Kumar, M. E. Galassi, R. D. Rivarola, O. Fojón, C. Champion, J. Hanssen, H. Lekadir, P. F. Weck, and L. C. Tribedi, Phys. Rev. A **85**, 032711 (2012).
[83] H.-D. Betz, Rev. Mod. Phys. **44**, 465 (1972).
[84] E. C. Montenegro, S. A. Cruz, and C. Vargas-Aburto, Phys. Lett. A **92**, 195 (1982).
[85] G. Schiwietz and P. L. Grande, Nucl. Instrum. Methods Phys. Res. B **175-177**, 125 (2001).